

PET-Based Human Dosimetry of ^{18}F -Galacto-RGD, a New Radiotracer for Imaging $\alpha\text{v}\beta\text{3}$ Expression

Ambros J. Beer^{1,2}, Roland Haubner¹, Ingo Wolf¹, Michael Goebel³, Stephan Luderschmidt⁴, Markus Niemeyer⁵, Anca-Ligia Grosu⁶, Maria-Jose Martinez¹, Hans Jürgen Wester¹, Wolfgang A. Weber¹, and Markus Schwaiger¹

¹Department of Nuclear Medicine, Technische Universität München, Munich, Germany; ²Department of Radiology, Technische Universität München, Munich, Germany; ³Department of Orthopedic Surgery, Technische Universität München, Munich, Germany;

⁴Department of Dermatology, Technische Universität München, Munich, Germany; ⁵Department of Gynecology, Technische Universität München, Munich, Germany; and ⁶Department of Radiation Therapy, Technische Universität München, Munich, Germany

^{18}F -Galacto-RGD is a new tracer for PET imaging of $\alpha\text{v}\beta\text{3}$, a receptor involved in a variety of pathologic processes including angiogenesis and metastasis. Our aim was to study the dosimetry of ^{18}F -galacto-RGD in humans. **Methods:** Eighteen patients with various tumors (musculoskeletal tumors [$n = 10$], melanoma [$n = 5$], breast cancer [$n = 2$], or head and neck cancer [$n = 1$]) were examined. After injection of 133–200 MBq of ^{18}F -galacto-RGD, 3 consecutive emission scans from the thorax to the pelvis were acquired at 6.7 ± 2.9 , 35.6 ± 7.6 , and 70.4 ± 12.2 min after injection. Blood samples ($n = 4$) for metabolite analysis were taken 10, 30, and 120 min after injection. The OLINDA 1.0 program was used to estimate the absorbed radiation dose. **Results:** Reversed-phase high-performance liquid chromatography of serum revealed that more than 95% of tracer was intact up to 120 min after injection. ^{18}F -Galacto-RGD showed rapid clearance from the blood pool and primarily renal excretion. Background activity in lung and muscle tissue was low (percentage injected dose per liter at 71 min after injection, 0.56 ± 0.15 and 0.69 ± 0.25 , respectively). The calculated effective dose was 18.7 ± 2.4 $\mu\text{Sv}/\text{MBq}$, and the highest absorbed radiation dose was in the bladder wall (0.22 ± 0.03 mGy/MBq). **Conclusion:** ^{18}F -Galacto-RGD demonstrates high metabolic stability, a favorable biodistribution, and a low radiation dose. Consequently, this tracer can safely be used for noninvasive imaging of molecular processes involving the $\alpha\text{v}\beta\text{3}$ integrin and for the planning and monitoring of therapeutic approaches targeting $\alpha\text{v}\beta\text{3}$.

Key Words: ^{18}F -Galacto-RGD; $\alpha\text{v}\beta\text{3}$ expression; PET; dosimetry; whole-body biodistribution

J Nucl Med 2006; 47:763–769

The integrin $\alpha\text{v}\beta\text{3}$ is an important receptor affecting tumor growth, local invasiveness, and metastatic potential (1,2). Integrins are dimeric transmembrane glycoproteins mediating adhesion and migration of cells on a variety of extracellular matrix proteins. Specifically, $\alpha\text{v}\beta\text{3}$ is highly

expressed on activated endothelial cells during angiogenesis (3). The use of $\alpha\text{v}\beta\text{3}$ antagonists is currently being evaluated as a strategy for anticancer therapies (4). Therefore, noninvasive determination of $\alpha\text{v}\beta\text{3}$ expression would be of great importance for pretherapeutic recognition of those patients most amenable to $\alpha\text{v}\beta\text{3}$ -directed therapies and for the assessment of receptor expression during therapy.

Because many integrins, including $\alpha\text{v}\beta\text{3}$, bind to the tripeptide sequence arginine-glycine-aspartic acid (single letter code RGD) of different matrix proteins (5), several radiolabeled RGD peptides have been developed for SPECT and PET (6–8). The glycosylated cyclic pentapeptide ^{18}F -galacto-RGD resulted from tracer optimization based on the first-generation peptide [^{125}I]-3-iodo-DTyr⁴-cyclo(-Arg-Gly-Asp-DTyr-Val) (9). A murine $\alpha\text{v}\beta\text{3}$ -positive tumor model has already shown that ^{18}F -galacto-RGD has receptor-specific accumulation, high metabolic stability, predominantly renal elimination, and a high affinity and selectivity for the $\alpha\text{v}\beta\text{3}$ integrin in vitro (10). Radiation dose estimates from dynamic PET studies on New Zealand White rabbits suggested that the effective dose should be in the range of an ^{18}F -FDG PET scan (11). The present study was performed to estimate the associated radiation dose and to characterize the biodistribution and metabolic stability of ^{18}F -galacto-RGD in humans.

MATERIALS AND METHODS

Radiopharmaceutical Preparation

Synthesis of the labeling precursor and subsequent ^{18}F labeling were performed as described elsewhere (10,11).

Analysis of Metabolites in Blood Samples

Blood samples were collected 10, 30, and 120 min after tracer injection. Samples were centrifuged at 2,000 rotations per minute, and the supernatant was passed through a Sep-Pak C-18 cartridge (Waters). The cartridge was washed with 1 mL of phosphate-buffered saline and was eluted with 1 mL of acetonitrile that included 0.1% trifluoroacetic acid. The solvent was removed in vacuo, and 0.5 mL of phosphate-buffered saline was added before analysis using reversed-phase high-performance liquid chromatography (10%–50% acetonitrile and 0.1% trifluoroacetic acid; 20 min at a flow rate of 3 mL/min).

Received Dec. 19, 2005; revision accepted Jan. 24, 2006.

For correspondence or reprints contact: Ambros J. Beer, Department of Nuclear Medicine, Technische Universität München, Klinikum rechts der Isar, Ismaninger Strasse 22, 81675 Munich, Germany.
E-mail: beer@roe.med.tum.de

Patients

The study was approved by the ethics committee of the Technische Universität München and the local radiation protection authorities. Informed written consent was obtained from all patients. Eighteen patients (11 women and 7 men; mean age \pm SD, 50.8 ± 17.8 y; range, 31–89 y), with diseases of the musculoskeletal system ($n = 10$), melanoma ($n = 5$), breast cancer ($n = 2$), or head and neck cancer ($n = 1$), were included in the study from September 2003 until April 2005 (Table 1). Diagnosis was confirmed by histopathology in 17 cases. In 1 case of metastasized melanoma, the diagnosis was based on clinical and imaging findings (contrast-enhanced CT of the thorax, abdomen, and pelvis and ^{18}F -FDG PET). In all patients with lesions of the musculoskeletal system, MRI of the tumor region was performed. For patients with melanoma, ^{18}F -FDG PET was performed in 4 cases and contrast-enhanced CT in 3 cases. All patients with breast cancer underwent mammography and breast ultrasound, and 1 patient underwent MRI mammography as well. In the patient with head and neck cancer, MRI and contrast-enhanced CT of the head and neck were performed. Inclusion criteria consisted of known or suspected malignancy, age over 18 y, and the ability to give written and informed consent. Exclusion criteria consisted of pregnancy, lactation, and impaired renal function (serum creatinine level > 1.2 mg/dL).

PET Procedure

Imaging was performed with an ECAT EXACT PET scanner (CTI/Siemens). The patients urinated before the examination and did not urinate between scans. Before injection of ^{18}F -galacto-RGD (133–200 MBq), a segmented transmission scan was acquired for 5 min per bed position (5 bed positions) using 3 rotating ^{68}Ge rod sources (each with approximately 90 MBq of ^{68}Ge) followed by 3 consecutive static emission scans in 2-dimensional mode beginning 5 min after tracer injection and covering the thorax to the pelvis (5–7

bed positions, 5 min per bed position). The field of view was 15.5 cm with overlapping acquisitions, resulting in a length of 13.6 cm for each bed position. The mean starting times for these emissions scans were 6.7 ± 2.9 , 35.6 ± 7.6 , and 70.4 ± 12.2 min after injection. Scanning was performed in the caudocranial direction.

Image Analysis and Dosimetry

Positron emission data were reconstructed using the ordered-subsets expectation maximization algorithm. Reconstructions were performed with 8 iterations and 4 subsets. The images were corrected for attenuation using the transmission data collected over the same region as for emission imaging. For image analysis, CAPP software, version 7.1 (CTI/Siemens), was used. Images were calibrated to Bq/mL for radiation dosimetry estimates.

An experienced operator placed regions of interest (ROIs) over major organs (lung, left ventricle, liver, spleen, intestine, kidneys, bladder, muscle, and breast) on 3 adjacent slices of the static emission scans. Because no substantial tracer accumulation was noted in the red bone marrow, no ROI could be drawn. The diameter of the ROIs was set to 2.5 cm, except for the kidney and intestine ROIs. There, polygonal ROIs adapted to the contour of the kidney or covering the area of maximum intestinal activity were drawn. For liver, spleen, and kidneys, we deliberately did not draw ROIs adapted to organ contours; doing so might have underestimated organ activity because of partial-volume effects. These effects can be avoided by placing an ROI of sufficient diameter in the center of the organ. Because of the limited number of time points at which measurements were obtained, a monoexponential fit was used for calculation of organ residence times (12,13).

For dosimetry calculations, the OLINDA 1.0 software (Vanderbilt University (14)) was used. Activity in the source organs was determined by multiplying the measured concentration (Bq/mL) by the organ masses of the OLINDA adult phantom. This

TABLE 1
Patient Data

Patient no.	Diagnosis	Sex	Age (y)	Weight (kg)	Injected activity (MBq)	Time after injection (min)		
						ES 1	ES 2	ES 3
1	Melanoma	M	56	75	144.30	5	32	60
2	Melanoma	M	44	72	214.60	5	28	58
3	Osteomyelitis	F	37	83	166.50	5	30	62
4	Melanoma	F	89	50	144.30	5	28	51
5	Chondrosarcoma	M	26	65	136.90	5	53	90
6	PVNS	F	31	68	125.80	12	42	75
7	Melanoma	F	59	53	188.70	5	30	62
8	Melanoma	M	36	60	155.40	6	33	94
9	Osseous metastasis	F	55	70	151.70	7	30	77
10	SCC, soft palate	M	50	50	173.90	5	31	60
11	Osseous metastasis	F	65	79	188.70	5	34	76
12	Osteosarcoma	M	35	52	172.05	12	42	75
13	Liposarcoma	M	51	108	173.90	4	41	83
14	PVNS	F	66	80	207.20	12	49	83
15	Osteosarcoma	F	41	57	189.81	12	46	78
16	Breast cancer	F	68	75	182.04	5	28	54
17	Liposarcoma	F	84	59	178.71	5	31	60
18	Breast cancer	F	38	63	184.26	5	32	69
Mean			51.72	67.72	171.04	6.67	35.56	70.39
SD			17.26	14.21	23.37	2.91	7.62	12.25

ES = emission scan; SCC = squamous cell carcinoma; PVNS = pigmented villonodular synovitis.

activity was expressed as percentage injected dose and plotted against time. Thus, the dose factors given here are dose factors for the reference man or woman, allowing easy comparison of our results with those of other dosimetric studies using this approach (15–17). Moreover, only about 5% of body weight is amenable to volumetry by using, for example, CT or PET datasets (liver, spleen, kidneys). For the patient with the highest body weight (patient 13), we compared dosimetry results obtained using, on the one hand, organ weights from the OLINDA adult phantom with those obtained using, on the other hand, organ weights from individual volumetry based on CT datasets (liver, spleen, kidneys). The effective dose was determined to be 16.8 $\mu\text{Sv}/\text{MBq}$ using the individual organ masses and 17.0 $\mu\text{Sv}/\text{MBq}$ using the organ masses from the adult phantom—a difference of only 1.2%. However, this example is just illustrative and the results cannot be generalized.

Bladder activity was determined as follows. Activity concentration was determined from 3 adjacent ROIs at least 2.5 cm in diameter drawn inside the bladder. Subsequently, the bladder volume was measured by drawing freehand ROIs around the bladder contour, with the images scaled to the maximum activity in the bladder. The volume was then calculated by the CAPP software. The mean bladder volume for the last emission scan at 70.4 min after injection was 491 ± 286 mL. Averaged data were fitted to an exponential rise to maximum, from which the total fraction of activity entering the bladder was derived. The total percentage of activity entering the bladder based on these results was estimated to be 71.2% ($\pm 31.5\%$). The biologic half-life was determined from whole-body effective half-life using various

voiding intervals (120, 60, and 30 min). Both values were entered in the dynamic bladder model of the OLINDA 1.0 program to determine the bladder-content residence time.

The gastrointestinal tract model of the OLINDA software was used to estimate hepatobiliary tracer elimination. The fraction of activity entering the intestine was determined by multiplying the measured small-intestine activity concentration by the standard mass of the small intestine. For calculation of total-body half-life, the total-body activity of each emission scan was determined by using the open-source software AMIDE 0.8, and the bladder activity was subtracted (18). A monoexponential fit was then applied to calculate the residence time for the total body. The residence time for the remainder of the body was calculated by subtracting organ and bladder residence times from the whole-body residence time.

RESULTS

Analysis of metabolites in blood samples ($n = 4$) using reversed-phase high-performance liquid chromatography showed that more than 95% of the tracer was intact at 120 min after injection.

Table 2 lists the average absorbed radiation dose for all organs using the individual organ residence times. Average residence times are listed in Table 3. The maximum residence time for ^{18}F is 2.64 h, and the sum of the mean residence times is 1.15 h. The difference accounts for activity

TABLE 2
Radiation Dose Estimates for Intravenous Administration of ^{18}F -Galacto-RGD

Site	All patients		Women		Men	
	Mean	SD	Mean	SD	Mean	SD
Adrenals	5.41	1.06	6.16	0.85	4.65	0.62
Brain	1.45	0.95	1.69	1.19	1.22	0.52
Breasts	1.99	0.74	2.32	0.84	1.61	0.30
Gallbladder wall	7.55	1.31	8.56	0.98	6.55	0.68
Lower large intestine wall	11.99	2.29	13.33	2.36	10.66	1.19
Small intestine	15.43	5.87	18.14	6.56	12.72	3.35
Stomach	4.13	0.98	4.71	0.99	3.55	0.52
Upper large intestine wall	16.28	6.65	19.12	7.59	13.43	3.83
Heart wall	3.53	0.94	4.08	0.98	2.98	0.45
Kidneys	29.52	11.95	31.99	7.18	27.06	14.90
Liver	23.04	7.82	26.81	9.44	19.26	2.19
Lungs	6.62	3.19	7.69	3.20	5.55	2.80
Muscle	5.26	0.99	5.76	0.91	4.76	0.78
Ovaries	11.07	1.46	11.07	1.46		
Pancreas	5.37	1.06	6.10	0.92	4.64	0.59
Red marrow	3.87	0.84	4.33	0.89	3.41	0.44
Bone surfaces	3.81	1.42	4.36	1.72	3.25	0.70
Skin	2.27	0.65	2.52	0.77	2.02	0.33
Spleen	16.30	4.20	18.89	3.67	13.71	2.91
Testes	4.44	2.26			5.50	0.46
Thymus	2.54	0.87	2.89	1.04	2.19	0.42
Thyroid	2.09	0.83	2.28	1.04	1.91	0.46
Urinary bladder wall	218.36	34.70	240.57	37.69	196.14	0.35
Uterus	17.37	1.50	17.37	1.50		
Total body	5.34	0.91	5.92	0.86	4.76	0.51
Effective dose ($\mu\text{Sv}/\text{MBq}$)	18.68	2.42	20.24	2.50	17.11	0.72

Data are $\mu\text{Gy}/\text{MBq}$.

TABLE 3
Mean Organ Residence Times of All Patients

Site	Mean	SD
Lower large intestine	0.39	0.13
Small intestine	3.78	1.41
Upper large intestine	2.07	0.79
Kidneys	3.99	1.96
Liver	15.20	4.42
Lungs	2.16	1.70
Muscle	27.88	8.10
Spleen	1.20	0.29
Bladder	41.0	0.00
Remainder	17.17	9.90

Data are (MBq × h/MBq) × 10².

excreted via the kidneys during a voiding interval of 2 h. The effective total-body half-life was 46 ± 12 min. For the 2-h voiding interval, the effective absorbed radiation dose was 18.7 ± 2.4 $\mu\text{Sv}/\text{MBq}$ (17.1 ± 0.7 $\mu\text{Sv}/\text{MBq}$ for men and 20.2 ± 2.5 $\mu\text{Sv}/\text{MBq}$ for women), with the highest absorbed dose— 0.22 ± 0.03 mGy/MBq—being in the bladder wall. Other organs with relatively high doses were the kidneys, liver, small intestine, and lungs. We also calculated the average absorbed radiation dose for a 1-h voiding interval and a 30-min voiding interval. For these intervals, the effective radiation doses were 12.7 ± 2.2 and 9.5 ± 1.7 $\mu\text{Sv}/\text{MBq}$, respectively. Again, the highest absorbed doses were in the bladder wall (0.11 ± 0.02 and 0.06 ± 0.01 mGy/MBq, respectively). Figure 1 shows representative dy-

namic coronal images acquired at 5, 33, and 62 min after tracer injection.

Figure 2 summarizes the percentage injected dose per liter for the various organs measured in the emission scans and averaged over all patients. The organ time–activity curves of a representative patient are shown in Figure 3. In general, the areas of highest activity were the urogenital tract (kidneys, ureter, and bladder), followed by the liver, spleen, and gut. Blood-pool activity was only moderate and declined over time. Background activity in the muscles and lungs was low. We observed no significant tracer accumulation in the gut during the examination period, and the fraction of activity entering the gastrointestinal tract was calculated to be $3.0\% \pm 1.7\%$. This finding confirms that the tracer was predominantly excreted via the renal pathway.

DISCUSSION

In this paper, we have described the dosimetry of the $\alpha\beta\beta$ -selective tracer ^{18}F -galacto-RGD in humans. The radiation dose is similar to that of ^{18}F -FDG. The tracer shows predominantly renal elimination and low background activity in most organs. These findings suggest that ^{18}F -galacto-RGD can safely and effectively be used for imaging $\alpha\beta\beta$ expression in humans.

The dosimetry calculations revealed the effective dose to be $18.7 \mu\text{Sv}/\text{MBq}$ and the bladder to be the critical organ, receiving the highest absorbed radiation dose ($218 \mu\text{Gy}/\text{MBq}$). Other organs receiving relatively high doses were the kidneys, spleen, liver, and small and large intestines. However, the dose to the intestine did not seem to be caused by hepatobiliary excretion, because the activity did

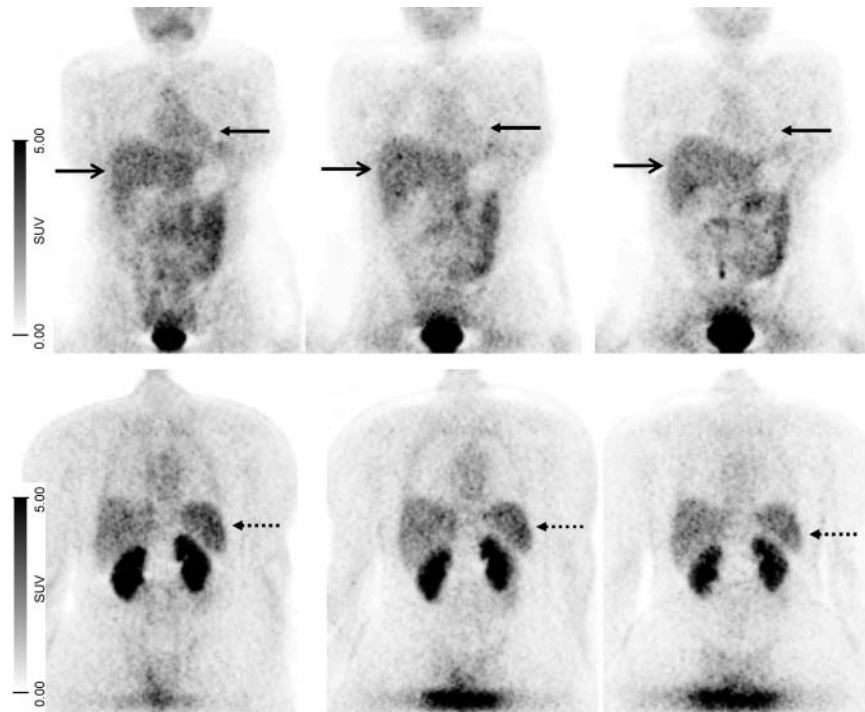


FIGURE 1. Static ^{18}F -galacto-RGD emission scans of 37-y-old woman at (from left to right) 5, 33, and 62 min after injection, with representative coronal views at level of heart and liver (top) and at level of kidneys (bottom). Blood pool (heart, upper solid arrow) shows rapid elimination of tracer, liver (lower solid arrow) shows moderate activity slowly decreasing over time, and spleen (dashed arrow) shows initially high activity decreasing over time.

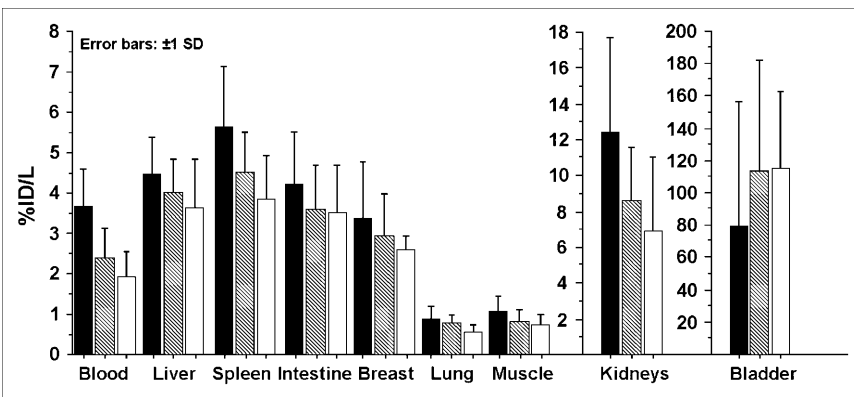


FIGURE 2. Mean percentage injected dose per liter, and SD, for major organs and muscle tissue determined on the basis of 3 static emission scans corrected for decay. Solid bar = 6 min after injection; hatched bar = 36 min after injection; open bar = 71 min after injection.

not increase over time. Therefore, we suggest that there might be a specific uptake in the bowel wall, perhaps due to $\alpha v\beta 3$ expression on intestinal smooth muscle cells (19). However, the absorbed dose for all these organs is considerably lower than that to the bladder wall (12–30 $\mu\text{Gy}/\text{MBq}$). The radiation dose estimates from our study correspond well with the estimates from our animal study on New Zealand White rabbits and mice (11). The animal study also showed that renal elimination of the tracer was fast, that tracer was not retained in any investigated organs, and that activity was highest in the bladder, at 60 min after injection. The radiation dose estimated for an adult female patient from the results of the animal study with New Zealand White rabbits was 0.22 $\mu\text{Sv}/\text{MBq}$ and therefore similar to the results of our current study (0.20 $\mu\text{Sv}/\text{MBq}$). In both the animal study and the human study, the bladder proved to be the critical organ. However, the estimated dose to the large intestine in the mouse model and, to a lesser extent, in the rabbit model was substantially higher than that found using our current data (mouse data, 0.082 mGy/MBq ; rabbit data, 0.028 mGy/MBq ; human data, 0.019 mGy/MBq). On the other hand, the estimated dose to the liver using mouse data and rabbit data was lower than that found using human data (mouse data, 0.010 mGy/MBq ;

rabbit data, 0.016 mGy/MBq ; human data, 0.027 mGy/MBq). This result probably reflects slower excretion kinetics and higher tracer retention in the liver in larger animals than in small animals.

The dose factors we calculated were those for the reference man or woman—a routine approach in dosimetric studies of new PET tracers (15–17). It was not our intention to calculate doses using the individual organ or body masses of our patients, because these values cannot be directly compared with published dose estimates for other compounds. Moreover, only about 5% of body weight is amenable to volumetry by using, for example, CT or PET datasets (liver, spleen, kidneys). However, if RGD peptides were to be used for radionuclide therapy, individual dosimetry based on the volumetry of individual organ masses would of course be essential. The total effective dose of ^{18}F -galacto-RGD according to our results is in the range of commonly applied oncologic radiotracers, such as ^{18}F -FDG (approximately 19.0 $\mu\text{Sv}/\text{MBq}$) (20,21). Even with the maximum amount of tracer (200 MBq of ^{18}F -galacto-RGD) injected in our study, a patient would be exposed to an effective dose of not more than 3.7 mSv. Using a higher—400-MBq—activity, similar to ^{18}F -FDG PET, to improve image quality would result in an effective dose of 7.4 mSv, which still corresponds

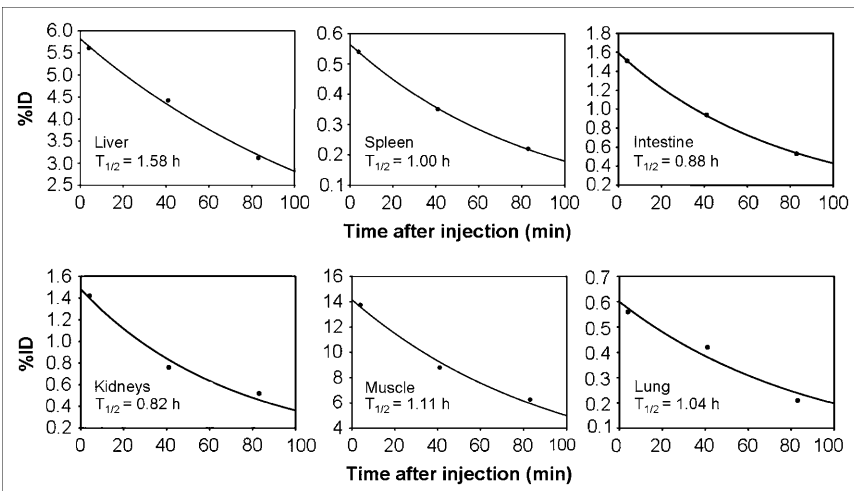


FIGURE 3. Organ time-activity curves and corresponding effective half-times for ^{18}F -galacto-RGD in patient 3. Graphs indicate percentage of total injected activity in each organ vs. time after injection of ^{18}F -galacto-RGD.

to risk category IIb as defined by the International Commission on Radiological Protection (minor to intermediate level of risk, appropriate for intermediate to moderate societal benefit) (22). Moreover, the absorbed dose could be reduced further by lowering the rather long voiding interval in our scenario from 2 to 1 h, assuming that for routine applications of ^{18}F -galacto-RGD, only 1 static emission scan at 60 min after injection would be necessary. For this scenario, we calculated a lower effective dose of 12.7 $\mu\text{Sv}/\text{MBq}$. Use of a diuretic agent such as furosemide could further decrease the absorbed dose of the bladder wall and probably would reduce the voiding interval to 30 min, resulting again in a markedly reduced effective dose compared with the 2-h voiding interval (effective dose, 9.5 $\mu\text{Sv}/\text{MBq}$). Image quality in the pelvis adjacent to the bladder would probably also improve, because the concentration of tracer in the bladder should be markedly reduced. This protocol (application of furosemide, 1 static emission scan at 60 min after injection) would be similar to the protocol used for ^{18}F -FDG PET in our institution, which is well tolerated by most of our patients. Moreover, bladder catheterization with continuous drainage could further reduce the radiation burden to the urinary tract.

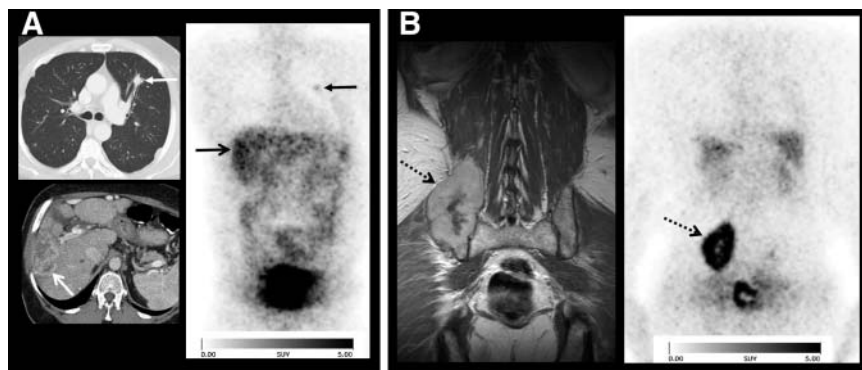
The biodistribution data for ^{18}F -galacto-RGD showed that the primary route of clearance is renal, with high tracer accumulation in the kidneys and especially in the bladder. Because of the high activity in the urine, image quality adjacent to the urinary tract and bladder was slightly impaired. The background activity in muscle tissue and the blood pool was low and decreased further over time. On the basis of these biodistribution patterns, imaging of $\alpha\text{v}\beta 3$ expression with ^{18}F -galacto-RGD is possible in the thorax, abdomen, and extremities, except for the urogenital tract. In the liver, spleen, and intestine, detection of lesions with only moderate tracer uptake might be impaired because of the higher background activity in these organs. Image quality in the pelvis might also be impaired by artifacts due to the high bladder activity (Fig. 4).

The integrin $\alpha\text{v}\beta 3$ plays a critical role in regulating tumor growth and angiogenesis and is significantly upregulated in sprouting tumor vessels and the cells of various tumors (23,24). Therefore, the noninvasive visualization and quantification of $\alpha\text{v}\beta 3$ -integrin levels in patients would allow a variety of possible applications. One potential application would be to document the $\alpha\text{v}\beta 3$ expression of tumors before therapy with $\alpha\text{v}\beta 3$ antagonists. Initial results from our patient study showed large inter- and intraindividual variances of ^{18}F -galacto-RGD accumulation in cancer patients (25,26). Patients with low or lack of $\alpha\text{v}\beta 3$ expression may not benefit from $\alpha\text{v}\beta 3$ antagonists and could receive an alternative therapeutic regimen. In patients with $\alpha\text{v}\beta 3$ -positive lesions, ^{18}F -galacto-RGD might be used to assess inhibition of the $\alpha\text{v}\beta 3$ integrin to optimize the dose of $\alpha\text{v}\beta 3$ antagonists. $\alpha\text{v}\beta 3$ expression has also been reported to be an important prognostic factor in tumors such as breast and colon cancer (27,28). Therefore, ^{18}F -galacto-RGD might be used to noninvasively characterize the biologic aggressiveness of a malignant tumor in an individual patient. Moreover, the noninvasive determination of $\alpha\text{v}\beta 3$ expression might be used as a surrogate parameter of angiogenesis in tumors that express this integrin only on endothelial cells and not on tumor cells. Recent data also suggest that it is possible to assess $\alpha\text{v}\beta 3$ expression in inflammatory processes using ^{18}F -galacto-RGD (29).

There are potential limitations to our study. Because our study, like many other dosimetric studies of new tracers, investigated patients rather than healthy volunteers, data from only 3 time points were used for calculation of residence times. More than 90 min without voiding would not have been tolerated by most of our patients unless the bladder had been catheterized. Also, no dynamic scans were obtained in this study, because we favored static emission scans of diagnostic quality with longer scans at each time point, consequently reducing the temporal resolution. Moreover, we cannot exclude the possibility that some tracer elimination to the bowel might have become notable because of the longer measurement periods. However, the advantage of a patient study is that the population under investigation is more representative of the future patient collective that would be investigated with ^{18}F -galacto-RGD.

The integrin $\alpha\text{v}\beta 3$ plays a critical role in regulating tumor growth and angiogenesis and is significantly upregulated in sprouting tumor vessels and the cells of various tumors (23,24). Therefore, the noninvasive visualization and quantification of $\alpha\text{v}\beta 3$ -integrin levels in patients would allow a variety of possible applications. One potential application would be to document the $\alpha\text{v}\beta 3$ expression of tumors before therapy with $\alpha\text{v}\beta 3$ antagonists. Initial results from our patient study showed large inter- and intraindividual variances of ^{18}F -galacto-RGD accumulation in cancer patients (25,26). Patients with low or lack of $\alpha\text{v}\beta 3$ expression may not benefit from $\alpha\text{v}\beta 3$ antagonists and could receive an alternative therapeutic regimen. In patients with $\alpha\text{v}\beta 3$ -positive lesions, ^{18}F -galacto-RGD might be used to assess inhibition of the $\alpha\text{v}\beta 3$ integrin to optimize the dose of $\alpha\text{v}\beta 3$ antagonists. $\alpha\text{v}\beta 3$ expression has also been reported to be an important prognostic factor in tumors such as breast and colon cancer (27,28). Therefore, ^{18}F -galacto-RGD might be used to noninvasively characterize the biologic aggressiveness of a malignant tumor in an individual patient. Moreover, the noninvasive determination of $\alpha\text{v}\beta 3$ expression might be used as a surrogate parameter of angiogenesis in tumors that express this integrin only on endothelial cells and not on tumor cells. Recent data also suggest that it is possible to assess $\alpha\text{v}\beta 3$ expression in inflammatory processes using ^{18}F -galacto-RGD (29).

FIGURE 4. 65-y-old man with hepatocellular carcinoma metastatic to lung and iliac bone. (A) Images of primary tumor (upper arrows) and of lung metastasis (lower arrows) include ^{18}F -galacto-RGD scan obtained 76 min after injection (right) and CT scans at levels of lungs (top left) and liver (bottom left). (B) Images of large osseous metastasis (arrows) in right iliac bone include ^{18}F -galacto-RGD scan obtained 76 min after injection (right) and T1-weighted coronal MRI scan obtained with intravenous gadolinium-diethylenetriami-nepentaacetic acid (left). Hepatocellular carcinoma is barely visible because of low lesion-to-background contrast in liver, whereas lesions in lung and bone are well demarcated. Hepatocellular carcinoma shows only intermediate tracer uptake (standardized uptake value, 2.9), compared with osseous lesion (standardized uptake value, 6.2), indicating lower $\alpha\text{v}\beta 3$ expression in primary tumor than in metastasis.



CONCLUSION

¹⁸F-Galacto-RGD demonstrates a radiation dose comparable to that of ¹⁸F-FDG and therefore can safely be used for imaging $\alpha v\beta 3$ expression. Because of the predominantly renal excretion of ¹⁸F-galacto-RGD, the effective dose could be further reduced by applying diuretic agents and by reducing the voiding interval.

ACKNOWLEDGMENTS

We thank Wolfgang Linke, Janette Carlsen, and the RDS-Cyclotron and PET team, especially Michael Herz, Petra Watzlowick, Gitti Dzewas, Coletta Kruschke, and Nikola Henke. The Münchner Medizinische Wochenzeitschrift and the Sander Foundation (grant 96.017.3) are acknowledged for financial support.

REFERENCES

- Hood JD, Cheresh DA. Role of integrins in cell invasion and migration. *Nat Rev Cancer*. 2002;2:91–100.
- Ruoslahti E. Specialization of tumor vasculature. *Nat Rev Cancer*. 2002;2:83–90.
- Brooks PC, Montgomery AM, Rosenfeld M, et al. Integrin alpha v beta 3 antagonists promote tumor regression by inducing apoptosis of angiogenic blood vessels. *Cell*. 1994;79:1157–1164.
- Dredge K, Dalgleish AG, Marriott JB. Recent developments in antiangiogenic therapies. *Expert Opin Biol Ther*. 2002;2:953–966.
- Ruoslahti E, Pierschbacher MD. New perspectives in cell adhesion: RGD and integrins. *Science*. 1987;238:491–497.
- Aumailley M, Gurrath M, Muller G, et al. Arg-Gly-Asp constrained within cyclic pentapeptides: strong and selective inhibitors of cell adhesion to vitronectin and laminin fragment P1. *FEBS Lett*. 1991;291:50–54.
- Haubner RH, Wester HJ, Weber WA, Schweiger M. Radiotracer based strategies to image angiogenesis. *Q J Nucl Med*. 2003;47:189–199.
- Haubner R, Wester HJ. Radiolabeled tracer for imaging of tumor angiogenesis and evaluation of anti-angiogenic therapies. *Curr Pharm Des*. 2004;10:1439–1455.
- Haubner R, Wester HJ, Reuning U, et al. Radiolabeled $\alpha v\beta 3$ integrin antagonists: a new class of tracers for tumor targeting. *J Nucl Med*. 1999;40:1061–1071.
- Haubner R, Wester HJ, Weber WA, et al. Noninvasive imaging of alpha(v)beta3 integrin expression using ¹⁸F-labeled RGD-containing glycopeptide and positron emission tomography. *Cancer Res*. 2001;61:1781–1785.
- Haubner R, Kuhnast B, Mang C, et al. [¹⁸F]Galacto-RGD: synthesis, radio-labelling, metabolic stability and radiation dose estimates. *Bioconjugate Chem*. 2004;15:61–69.
- Ribeiro M, Ricard M, Bourgeois S, et al. Biodistribution and radiation dosimetry of [¹¹C]raclopride in healthy volunteers. *Eur J Nucl Med Mol Imaging*. 2005;32:952–958.
- Bottlaender M, Valette H, Roumenov D, et al. Biodistribution and radiation dosimetry of ¹⁸F-fluoro-A85380 in healthy volunteers. *J Nucl Med*. 2003;44:596–601.
- Stabin MG, Sparks RB, Crowe E. OLINDA/EXM: the second-generation personal computer software for internal dose assessment in nuclear medicine. *J Nucl Med*. 2005;46:1023–1027.
- Vesselle H, Grierson J, Peterson BA, Muzi M, Mankoff DA, Krohn KA. ¹⁸F-Fluorothymidine radiation dosimetry in human PET imaging studies. *J Nucl Med*. 2003;44:1482–1488.
- Yaghoubi S, Barrio JR, Dahlbom M, et al. Human pharmacokinetic and dosimetry studies of [¹⁸F]FFHBG: a reporter probe for imaging herpes simplex virus type-1 thymidine kinase reporter gene expression. *J Nucl Med*. 2001;42:1225–1234.
- Laforest R, Dehdashti F, Lewis JS, Schwarz SW. Dosimetry of ⁶⁰Co/⁶²Mn/⁶⁴Cu-ATSM: a hypoxia imaging agent for PET. *Eur J Nucl Med Mol Imaging*. 2005;32:764–770.
- Loening AM, Gambhir SS. AMIDE: a free software tool for multimodality medical image analysis. *Mol Imaging*. 2003;2:131–137.
- Kuemmerle JF. Occupation of alpha-v-beta-3 integrin by endogenous ligands modulates IGF-I receptor activation and proliferation of human intestinal smooth muscle. *Am J Physiol Gastrointest Liver Physiol*. September 29, 2005 [Epub ahead of print].
- Deloar HM, Fujiwara T, Shidahara M, et al. Estimation of absorbed dose for 2-[¹⁸F]fluoro-2-deoxy-D-glucose using whole body emission tomography and magnetic resonance imaging. *Eur J Nucl Med*. 1998;25:565–574.
- Deloar HM, Fujiwara T, Shidahara M, Nakamura T, Yamadera A, Itoh M. Internal absorbed dose estimation by a TLD method for ¹⁸F-FDG and comparison with dose estimates from whole body PET. *Phys Med Biol*. 1999;44:595–606.
- ICRP Publication 62: *Radiological Protection in Biomedical Research*. Oxford, U.K.: Pergamon Press; 1991:12.
- Cairns RA, Khokha R, Hill RP. Molecular mechanisms of tumor invasion and metastasis: an integrated review. *Curr Mol Med*. 2003;3:659–671.
- Felding-Habermann B. Integrin adhesion receptors in tumor metastasis. *Clin Exp Metastasis*. 2003;20:203–213.
- Haubner R, Weber WA, Beer AJ, et al. Non-invasive visualization of the activated $\alpha v\beta 3$ integrin in cancer patients by positron emission tomography and [¹⁸F]galacto-RGD. *PLoS Med*. 2005;2:e70.
- Beer AJ, Haubner R, Goebel M, et al. Biodistribution and pharmacokinetics of the $\alpha v\beta 3$ -selective tracer ¹⁸F-galacto-RGD in cancer patients. *J Nucl Med*. 2005;46:1333–1341.
- Gasparini G, Brooks PC, Biganzoli E, et al. Vascular integrin $\alpha v\beta 3$: a new prognostic indicator in breast cancer. *Clin Cancer Res*. 1998;4:2625–2634.
- Vonlaufen A, Wiedle G, Borisch B, Birrer S, Luder P, Imhof BA. Integrin $\alpha v\beta 3$ -expression in colon carcinoma correlates with survival. *Mod Pathol*. 2001;14:1126–1132.
- Pichler BJ, Kneilling M, Haubner R, et al. Imaging of delayed-type hypersensitivity reaction by PET and ¹⁸F-galacto-RGD. *J Nucl Med*. 2005;46:184–189.